A Solution Based Route to GaAs Thin Films from $As(NMe_2)_3$ and $GaMe_3$ for Solar Cells

Sanjayan Sathasivam,[a] Ranga R. Arnepalli,[b] Kaushal K. Singh,[b] Robert J. Visser,[b] Christopher S. Blackman,[a] Claire J. Carmalt[a]*

[a]Materials Chemistry Research Centre, Department of Chemistry, University College London, 20 Gordon Street, London, U.K. WC1H 0AJ

[b]Applied Materials Inc., 3225 Oakmead Village Drive, M/S 1240 P.O. Box 58039, Santa Clara, California 95052-8039, USA

Abstract

The novel deposition of GaAs thin films on glass substrates from a solution based route involving the aerosol assisted chemical vapour deposition (AACVD) of $As(NMe_2)_3$ and $GaMe_3$ dissolved in toluene is reported. The gallium arsenide films were analysed by scanning electron microscopy (SEM), X-ray powder diffraction (XRD), energy dispersive X-ray (EDX) analysis, X-ray photoelectron spectroscopy (XPS) and Raman spectroscopy. Powder XRD showed that cubic polycrystalline GaAs had been deposited with films grown at the higher temperatures having a Ga to As ratio of 1:1. EDX mapping, XPS depth profiling and SIMS showed that the films contained low levels of contaminants. The method described shows the formation of GaAs films with increasing crystallinity and stoichiometry reaching unity with increasing deposition temperature.

Keywords: gallium arsenide, AACVD, solution processing, photovoltaics

Introduction

The search for new routes to semiconducting materials continues to attract considerable attention, despite the many advances that have resulted in the semiconductor-based revolution in electronic devices.[1] The use of solution processes as a method to reduce processing costs for the development of electronic devices is attracting interest for a wide range of applications.[2,3] Gallium arsenide (GaAs) is a semiconductor with a direct band gap of 1.43 eV that finds applications in photovolatics and optoelectronic devices.[4,5] Recently, thin film GaAs solar devices have been reported with an efficiency of 28.8% which are superior to those achieved for silicon based devices (amorphous silicon - efficiency of 20.1%; crystalline silicon - 25.0%).[6] The greater device performance is a result of GaAs having high electron mobility and its resistance to heat and radiation.[4,7,8] Furthermore, the bandgap for GaAs is close to the optimum bandgap (1.34 eV) for solar conversion for a single junction solar cell.[9,10] Unfortunately, the high cost of fabricating GaAs devices has limited the use of GaAs photovoltaics to space and military applications only.

Formation of these devices currently involves epitaxial methods, including molecular beam epitaxy (MBE) and metal organic chemical vapour deposition (MOCVD), utilising expensive substrates such as germanium and GaAs. The deposition methods typically use dual source precursors, such as trimethylgallium ($GaMe_3$), which is a pyrophoric liquid and the highly toxic arsine gas, AsH_3.[11] Single-source precursors, including $[Me_2GaAs(H)^tBu]_2$,[12] $[R_2GaAs^tBu_2]_2$[13,14] and $[^nBu_2Ga(□\text{-}As^nBu_2)_2Ga^nBu_2]_2$[15] have been reported as potential alternatives to the dual source routes. Alternatively, different gallium and arsenic precursors have been studied. Carbon contamination from the arsenic precursor is a major problem when depositing GaAs films, hence trialkyl arsines are generally avoided as they are a source of carbon in the film. Alternatives to AsH_3 include liquid precursors, such as tertbutylarisne, which is still highly toxic, and tris(dimethylaminoarsine), $As(NMe_2)_3$.[16,17]

Tris(dimethylaminoarsine) is a liquid precursor that is used in many MOCVD techniques due to its low volatility and low relative decomposition temperature compared to tertbutyl arsine and arsine.[17] Furthermore, the precursor is lacking in carbon and hence is not a source of carbon contamination in the deposited films. For example, GaAs films have been grown with undetectable carbon levels at 450 ˚C using trimethylgallium as the gallium source via metal organic MBE.[18] The major

decomposition products of $As(NMe_2)_3$ have been found to be dimethylamine, hydrogen and aziridine.[19]

Here, we present the use of $As(NMe_2)_3$ with $GaMe_3$ in a simple solution-based, one-pot, technique to deposit GaAs thin films via aerosol assisted chemical vapour deposition (AACVD). The films were grown on glass and the deposition of GaAs on amorphous substrates is still relatively limited.[20,21] The AACVD technique is a solution based process which relies on the solubility of the precursors, rather than its volatility and control of the resulting morphology of the films can be achieved which can influence the properties of the resulting film.[22] This technique has been used to produce high quality films for electrical and optical applications.[22,23,24] AACVD operates at atmospheric pressure and therefore expensive equipment is not required. The one-pot route involving two commercially available precursors, $As(NMe_2)_3$ and $GaMe_3$, removes the need to isolate the precursor before deposition.

Experimental Section

Caution! Trimethylgallium and tris(dimethylamino)arsine are pyrophoric and must be handled in an inert atmosphere. In addition, tris(dimethylamino)arsine is toxic and must be handled with care. All experiments must be carried out in a fume cupboard.

Trimethylgallium (SAFC Hightech - 99.999%) and tris(dimethylamino)arsine (Strem Chemicals Inc. - 99%) was used as received. Toluene (Alfa Aesar) was dried (Anhydrous Engineering) and stored under alumina columns.

To form the precursor solution $As(NMe_2)_3$ (1.08 g, 5.2 mmol) was dissolved in toluene (10 mL) at -78 ˚C. $GaMe_3$ (0.4 g, 3.5 mmol) was dissolved in toluene (10 mL) at -78 ˚C. The $As(NMe_2)_3$ in toluene solution was added dropwise to the $GaMe_3$/toluene solution and the solution allowed to reach room temperature before deposition was carried out at 450, 500 and 550 ˚C.

The precursor solution for all AACVD depositions was placed in a glass bubbler and aerosolised by use of a Vicks ultrasonic humidifier (model number: 4022167500175). Nitrogen (BOC - 99.9%) carrier gas was used as supplied. Depositions were carried out on SiO_2 coated float-glass that was cleaned using petroleum ether (60-80 ˚C) and propan-2-ol and dried in air prior to use. The glass substrates were ca. 90 mm x 45 mm

x 4 mm in size. The heating of the glass substrate to the desired temperature was carried out under nitrogen gas and two-way taps were used to divert the nitrogen carrier gas through the bubbler. After all the precursor solution had passed through the chamber the taps were turned to allow only N_2 gas flow through the bypass tap. This was maintained until the reaction chamber temperature falls below 100 °C. The N_2 gas was stopped and the glass substrates were removed. The N_2 gas flow rate was controlled by a calibrated flow meter positioned before the gas enters the bypass bubbler. The total deposition time was in the region of 50 – 80 min.

A graphite block containing a Watlow cartridge heater was used to heat the glass substrate. The temperature of the substrate was monitored by a Pt–Rh thermocouple. Post deposition the films were safe to handle. Coated substrates were handled and stored in air. Large pieces of glass (ca. 4 cm x 2 cm) were used for X-ray powder diffraction but the coated substrate was cut into ca. 1 cm x 1 cm squares for subsequent analysis by SEM and EDX.

X-ray diffraction (XRD) was carried out using a microfocus Bruker GAADS powder X-ray diffractometer with a monochromated Cu K_α (1.5406 Å) source. Raman spectroscopy was performed using a Renishaw 1000 spectrometer equipped with a 514.5 nm laser. Energy dispersive X-ray spectroscopy was measured on a JOEL JSM-6301F Field Emission instrument with acceleration voltage of 20 kV, the Ga atom% was derived from Ga-K_α line (9243 eV) and the As atom% derived from the As K_α line (1053 eV). X-ray photoelectron spectroscopy (XPS) was carried out using a Thermo Scientific *K*-Alpha instrument with monochromatic Al-K_α source to identify the oxidation state and chemical constituents. High resolution scans were obtained for the Ga (3d), As (3d), O (1s) and C (1s) at a pass energy of 40 eV. The peaks were modelled using CasaXPS software with binding energies adjusted to adventitious carbon (284.5 eV). SEM images were taken on a JOEL JSM-6301F Field Emission instrument with acceleration voltage of 5 kV. Images were captured using SEMAfore software. For both SEM and EDX samples were cut to 10 mm x 10 mm coupons and coated with a fine layer of gold (SEM) and carbon (EDX) to avoid charging. HRTEM and EDX mapping was carried out on Titan 80-300 TEM with EDX at CAMCOR service at the University of Oregon. SIMS was carried out by Evans analytical group, Santa Clara, California.

Results and discussion

Polycrystalline thin films of GaAs were deposited on glass substrates from AACVD of $As(NMe_2)_3$ and $GaMe_3$ in toluene at 450, 500 and 550 °C with a carrier gas flow rate of 0.5 $Lmin^{-1}$. The two precursors were mixed at reduced temperature (-78 ˚C) and then allowed to warm to room temperature in the AACVD bubbler before the deposition was started. In order to achieve a stoichiometry close to GaAs in the resulting films a 1.5:1 ratio of $As(NMe_2)_3$: $GaMe_3$ was required (Table 1). Increasing the amount of $As(NMe_2)_3$ (greater than a 1.5:1 ratio) did not result in any change in film stoichiometry. The film grown at 450 °C was substoichiometric in spite of a 1.5:1 ratio of $As(NMe_2)_3$: $GaMe_3$ in the precursor solution.

The films deposited under these conditions were smooth, continuous and appeared grey/blue in colour under reflected light. They were adherent to the substrate, passing the Scotch Tape™ test but were scratched by stainless steel and brass stylus as expected for GaAs films. Electrical measurements carried out using a two-point probe revealed electrical resistance in the MΩ region therefore indicating the films were insulating at room temperature, as expected for pristine GaAs.[25]

Film	Temperature / °C	Toluene / mL	$As(NMe_2)_3$ / mmol	$GaMe_3$ / mmol	Gallium / Atm%	Arsenic / Atm%
1	450	20	5.2	3.5	63	37
2	500	20	5.2	3.5	54	46
3	550	20	5.2	3.5	52	48

Table 1: Conditions for the deposition of GaAs films on glass substrates and composition of the films from EDX.

Although the mechanism of the AACVD reaction was not studied in detail previous solution based studies have shown that the reaction of $As(NMe_2)_3$ and $GaMe_3$ results in initial formation of the adduct, $[GaMe_3\{As(NMe_2)_3\}]$, followed by ligand transfer forming species, of the type $[Me_2GaNMe_2]_2$, $[MeAsNMe_2]_2$ and $[GaMe_3\{AsMe(NMe_2)_2\}]$.[26] Similar observations have been also been reported for the reactions of $AlMe_3$ with Me_2AsNMe_2, $MeAs(NMe_2)_2$ and $As(NMe_2)_3$.[27,28] Therefore,

it is likely that similar reactions and ligand rearrangements are taking place in the AACVD bubbler prior to deposition.

All of the films showed only the formation of cubic polycrystalline GaAs (Figure 1), with peaks corresponding to cubic GaAs (111), (220) and (311) observed at 27.3°, 45.4°, and 53.7° 2θ respectively. The films grown at 450 ˚C were only very weakly diffracting, either due to the films being very thin or the temperature of 450 °C being too low to crystallise GaAs.

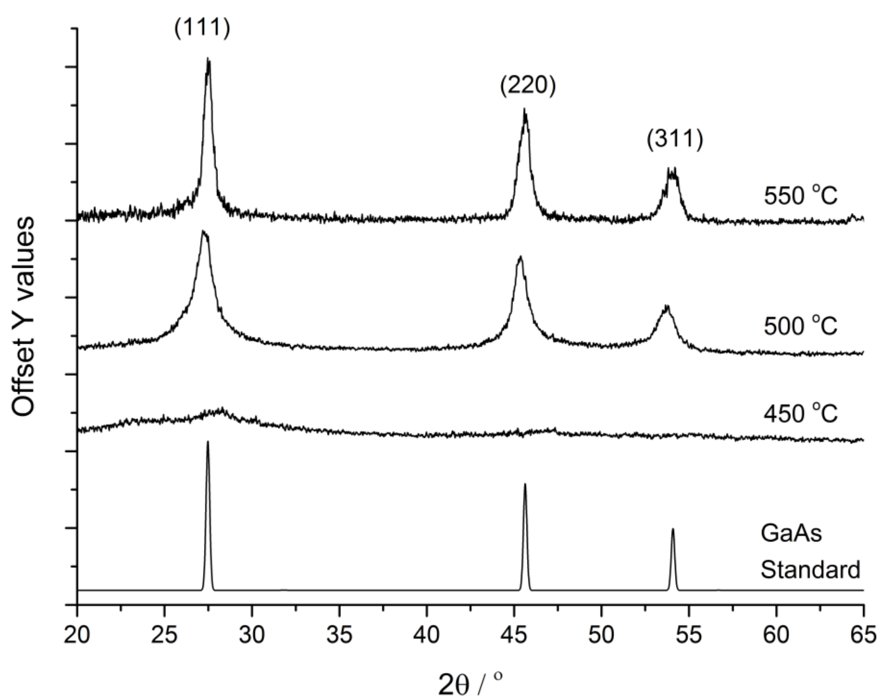

Figure 1: The XRD patterns for the GaAs films grown at 450 ˚C, 500 °C and 550 °C *via* the AACVD reaction of $As(NMe_2)_3$ and $GaMe_3$.

The films grown at 500 and 550 °C showed more intense diffraction peaks in the XRD pattern compared to those grown at 450 °C and an estimate of the crystallite size (Table 2) in each of the films calculated *via* the Scherrer equation,[29,30] showed that films grown at 550 °C had an average crystallite size (10 - 12 nm) twice as large as those grown at 500 °C (5 - 7 nm).

Film grown at 500 ˚C					
hkl	Bragg Angle / 2θ	Peak width /˚	Instrument resolution/˚	Corrected peak width /˚	Diameter /nm
111	27.5	1.84	0.08	1.76	5
220	45.8	1.21	0.055	1.155	7
311	54.2	1.68	0.065	1.615	6
Film grown at 550 ˚C					
hkl	Bragg Angle / 2θ	Peak width /˚	Instrument resolution/˚	Corrected peak width /˚	Diameter /nm
111	27.5	0.93	0.08	0.85	10
220	45.7	0.75	0.055	0.695	12
311	54.1	0.97	0.065	0.905	10

Table 2: The crystallite size of films grown at 500 and 550 ˚C.

Raman spectroscopy data showed the two bands expected for cubic GaAs (Figure 2) for all films. These are a longitudinal optical phonon mode at 274 cm^{-1} and a doubly degenerate transverse optical TO phonon mode at 253 cm^{-1}, which corresponds with literature values for bulk GaAs, although there is a red shift.[31] The deviation from the literature values could be due to strain in the GaAs lattice arising from growth of the films on amorphous glass substrates. In addition, the polycrystalline nature of the films has resulted in peak broadening due to the breakdown of the q=0 selection rules that occur when long ranger order (i.e. crystallinity) is lost.[32]

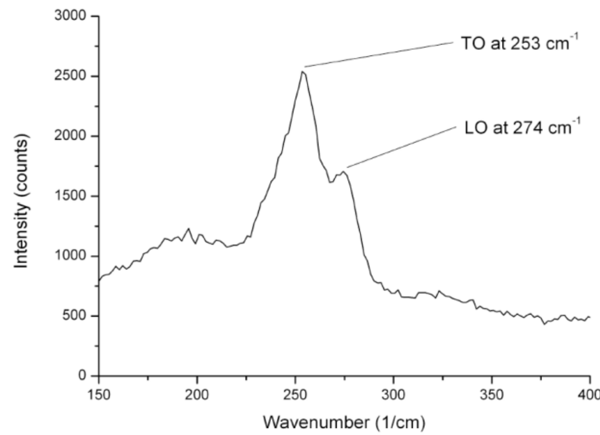

Figure 2: Raman spectrum of a GaAs film grown at 500 ºC.

In order to obtain compositional analysis of the resulting GaAs films, energy dispersive X-ray (EDX) analysis was used. EDX showed that the only elements present were gallium, arsenic and oxygen. The oxygen is likely due to contamination on the surface of the films due to the formation of a native oxide layer consisting of arsenic and gallium oxides (*vida supra*), which is a common on GaAs surfaces.[33] Films grown at 450 ˚C were non-stoichiometric (Table 1) with a gallium excess of ~25 atm%, however EDX analysis showed roughly equal amounts of Ga and As were present in the films grown at 500 and 550 ˚C.

EDX mapping (Figure 3) was carried out from the surface through to the substrate, which indicated that oxygen (and carbon) was indeed present mainly on the surface of the film (shown by the absence of colour in the figure). However, some oxygen was detected in the region near the substrate, where the arsenic content was also low, suggesting gallium oxide is present here. This maybe due to the diffusion of oxygen from the glass substrate into the film. The gallium to arsenic ratio was uniform throughout the bulk of the film indicating that Ga is only bound to As in the form of GaAs, except in the vicinity of the surface and the substrate.

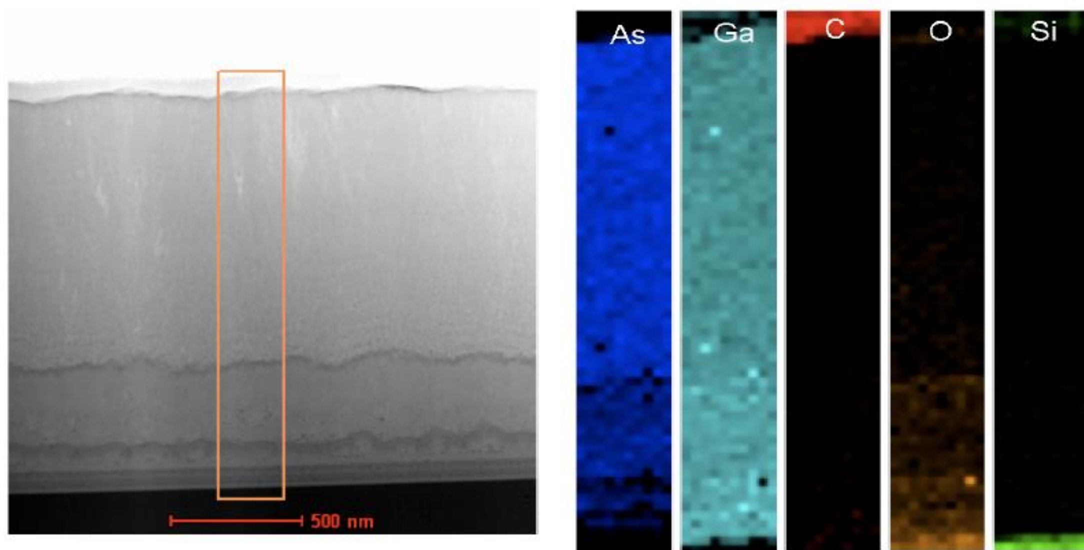

Figure 3: EDX mapping of a GaAs film grown at 500 ºC.

Scanning electron microscopy (SEM) was used to study the morphology of the GaAs films (Figure 4). SEM showed that the films were compact with featured morphology resulting from island type growth occurring in the deposition. At the higher temperature of 550 ˚C, SEM indicates the formation of larger and more defined

features (Figure 4 a,b). Side-on SEM was used to determine the thickness of the resulting films, the film deposited at 500 °C had a film thickness ranging between 1 to 2 μm whereas the 550 °C film was thicker at a range of 3 to 4 μm (see supporting information). A thickness gradient was observed such that the films were slightly thicker nearer to the inlet of the AACVD reactor

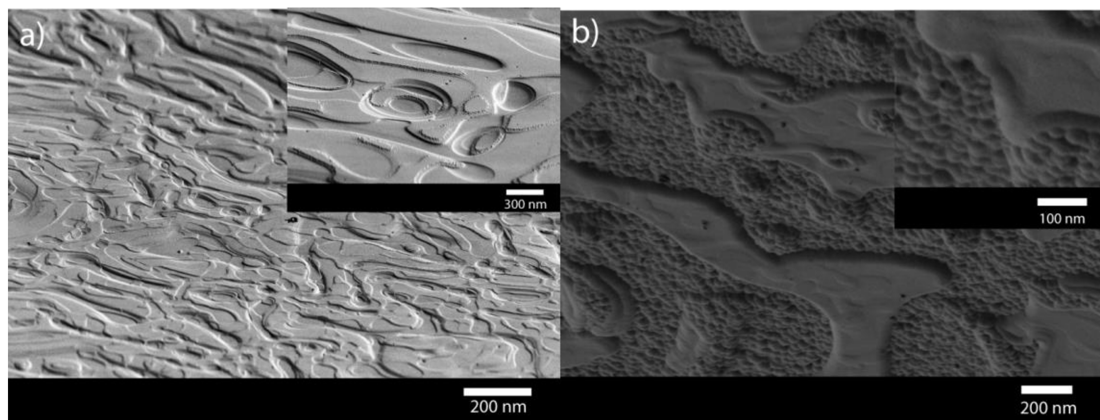

Figure 4: SEM images of the crystalline GaAs films grown *via* AACVD from $As(NMe_2)_3$ and $GaMe_3$ at a) 500 °C and b) 550 °C

The grain size distribution and polycrystallinity of the films was investigated using high-resolution transmission electron microscopy (HRTEM) (Figure 5). The darkfield HRTEM image (Figure 5d) suggests that there is minimum or no columnar growth since there was an absence of convex features on the top region of the film. This indicates that there are grain boundaries in both the vertical and lateral directions. Further evidence for this can be seen from the top down HRTEM image of the films, which shows the presence of grain boundaries typical of polycrystalline films (Figure 5a-c). Amorphous regions within the films were also observed in the top down HRTEM, especially near the glass substrate, as well as nanocrystalline GaAs in some regions of the film.

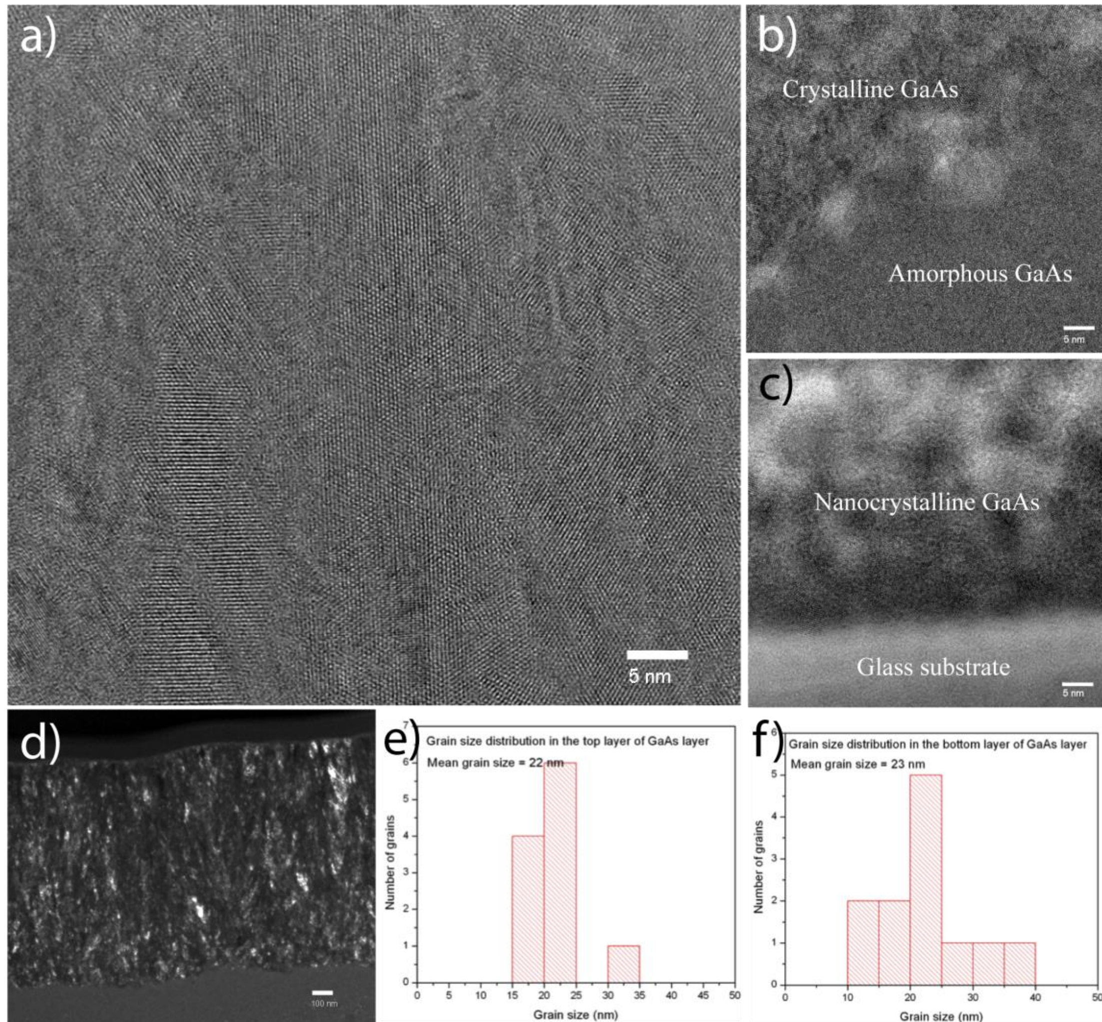

Figure 5: HRTEM data for GaAs films grown at 500 ˚C. (a) Darkfield TEM image of the film (b) top down TEM image (c) image showing nanocrystalline GaAs regions (d) image showing crystalline and amorphous GaAs regions (e) grain size distribution in the top region of the film (f) grain size distribution in the bottom region of the film.

The crystallite size distribution was calculated from the HRTEM data for both the bottom and top layers of the films, which were found to be similar (Figure 5e-f). The top layer of the films have an average crystallite size of 22 nm, whereas the bottom layer have an average size of 23 nm. It is worth noting that the crystallite size from HRTEM is larger than those obtained from the Scherrer equation – 6 nm (Table 2) which is not unexpected since the grain size estimation via the Scherrer equation has a larger error associated with it compared with direct determination methods, such as HRTEM.

X-ray photoelectron spectroscopy (XPS) was carried out on the films deposited at 500 ˚C to determine the extent of oxygen and carbon contamination within the depth of the film. XPS showed the presence of Ga, As, C and O. The Ga 3d peaks were

resolved to show the presence of two Ga^{3+} environments corresponding to GaAs at $3d_{5/2}$ binding energy of 19.7 eV and Ga_2O_3 $3d_{5/2}$ binding energy 20.8 eV. These match well with binding energy previously reported for GaAs and Ga_2O_3.[34,35] The As 3d peak was de-convoluted to three different As $3d_{5/2}$ and $3d_{3/2}$ peaks corresponding to As in the form of GaAs at 41.1 eV and AsO and As_2O_3 at 42.4 and 44.5 eV, respectively.[36] Three environments for the O 1s peak were observed, corresponding to Ga_2O_3 at 531.0 eV and As_2O_3 at 531.9 and 533.0 eV. These results are expected for the surface of GaAs, which is prone to the formation of the native oxide.

An XPS depth profiling study was carried out (Figure 6) and showed that the oxygen and carbon contamination is largely surface bound, as indicated by the EDX mapping and consistent with literature reports.[33] The oxide peak observed in the As 3d spectra disappears after 30 seconds of sputtering, showing that the oxygen is only surface contamination. The gallium peak corresponding to GaAs is the only peak observed after 30 seconds of sputtering, suggesting that the gallium oxide is surface segregated. From the EDX mapping, some oxygen contamination was observed near the bottom of the film by the substrate, although this was not observed in the XPS results presumably due to the sputtering not penetrating deep enough into the film even after 3000 seconds.

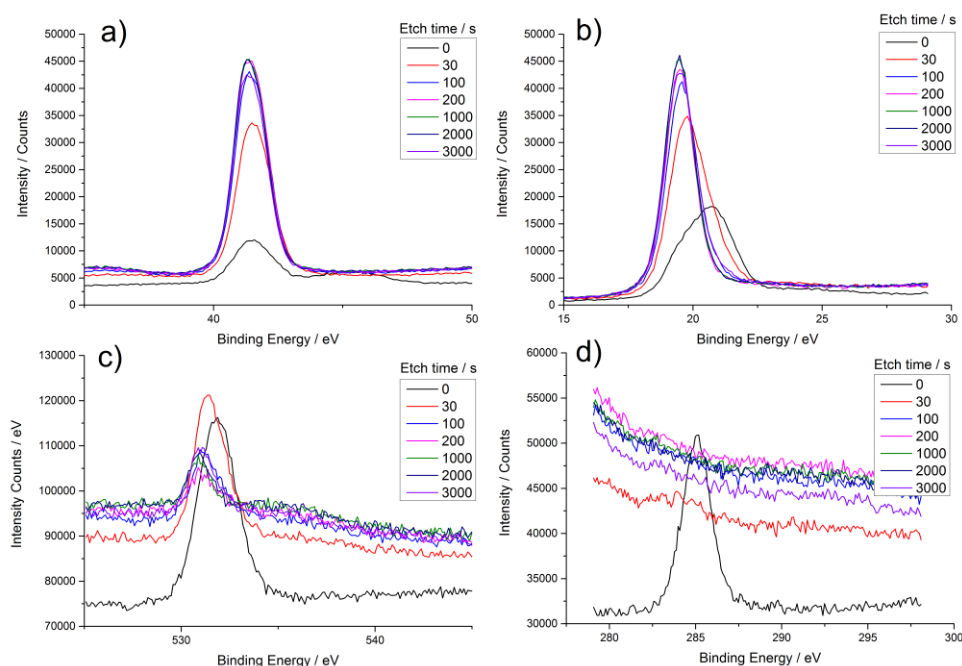

Figure 6: XPS depth profile of a) As 3d b) Ga 3d, c) O 1s, d) C 1s for the film grown via AACVD at 500 °C.

Secondary ion mass spectroscopy (SIMS) was carried out to determine any low level of oxygen or carbon contamination in the GaAs films. SIMS showed that for these films, the carbon concentration was 3.41 x 10^{20} atoms cm^{-3} and remains consistant through the film. The concentration of oxygen was found to be 4.66 x 10^{21} atoms cm^{-3} from the top surface to ~2.4 mm into the film. It then increases to 4.37 x 10^{23} atoms cm^{-3} when the substrate is reached due to diffusion of oxygen from the substrate.

These results are consistent with the EDX mapping and show that although the level of O and C are low they are too high for application in photovoltaic devices. Current work is investigating the reduction of C and O within the film as well as producing films with columnar growth for solar application. However, the method described herein involves a straightforward one-pot solution based technique that is easily scalable and the formation of GaAs films with good crystallinity and stoichiometry is possible.

Conclusions

The novel deposition of polycrystalline GaAs films on glass substrates has been achieved from the AACVD of a one-pot solution of commercially available presursors, $As(NMe_2)_3$ and $GaMe_3$ in toluene. Films were stoichiometric when the $As(NMe_2)_3$ and $GaMe_3$ ratio in the AACVD solution was 1.5 to 1 and were relatively low in carbon and oxygen contaminations as determined by cross sectional EDX mapping. SEM micrographs showed the films to have a structured morphology due to the high CVD growth rate. Further work is being undertaken in the group to reduce contamination and to produce films with less featured morphology that can be used for a photovoltaic device.

Acknowledgements

Applied Materials Inc. are thanked for funding and a studentship (SS). Dr. Ghazel Saheli is thanked for XPS depth profiling.

References

[1] M. Graetzel, R. A. J. Janssen, D. B. Mitzi, E. H. sargent, *Nature*, **2012**, 488, 304.

[2] A. C. Arias, J. D. Mackenzie, I. McCulloch, J. Rivnay, A. Salleo, *Chem. Rev.* **2010**, 110, 3.

[3] T. Shimoda, Y. Matsuki, M. Furusawa, T. Aoki, I. Yudasak, H. Tanaka, H. Iwasawa, D. Wang, M. Miyasaka, Y. Takeuchi, *Nature*, **2006**, 440, 783.

[4] J. S. Blakemore, *J. Appl. Phys.*, **1982**, 53, R123.

[5] W. W. Bett, F. Dimroth, G. Stollwerck, O. V. Sulima, *Appl. Phys. A*, **1999**, 69, 119.

[6] M. A. Green, K. Emery, Y. Hishikawa, W. Warta, E. D. Dunlop, *Prog. Photovolt; Res. Appl.*, **2013**, 21, 1.

[7] J. Yoon, S. Jo, I. S. Chun, I. Jung, H. S. Kim, M. Meitl, E. Menard, X. Li, J. J. Coleman, U. Paik, J. A. Rogers, *Nature*, **2010**, 465, 329.

[8] A. R. Gobat, M. F. Lamorte, G. W. McIver, *IRE Trans. Military Elec.*, **1962**, 20.

[9] C. W. Cheng, K. T. Shiu, N. Li, S. J. Han, L. Shi, D. K. Sadana, *Nat. Commun.*, **2013**, 4, 1577.

[10] W. Shockley, H. J. Queisser, *J. Appl. Phys.* **1961**, 32, 510.

[11] H. M. Manasevit, W. I. Simpson, *J. Electrochem Soc.*, **1969**, 116, 1725.

[12] S. Sathasivam, R. R. Arnepalli, K. Bhaskar, K. Singh, R. Visser, C. Blackman, C. J. Carmalt, *Chem. Mater.* 2014, submitted.

[13] A. H. Cowley, R. A. Jones, Angew. Chem., Int. Engl., **1989**, 75, 101.

[14] M. A. Arif, B. L. Benac, A. Cowley, R. Geerts, R. A. Jones, A. Jones, K. B. Kidd, C. M. Nunn, *J. Am. Chem. Soc*, **1988**, 110, 6248.

[15] F. Cheng, K. George, A. L. Hector, M. Jura, A. Kroner, W. Levason, J. Nesbitt, G. Reid, D. C. Smith, J. W. Wilson, Chem. Mater., **2011**, 23, 5217.

[16] M. A. Malik, M. Afzaal, P. O'Brien, *Chem. Rev.* **2010**, 110, 4417.

[17] C. J. Carmalt, S. Basharat, *Comprehensive Organometallic Chemistry III*, R. M. Crabtree and D. M. P. Mingos (Eds), **2007**, Volume 12, p1-34. Elsevier.

[18] D. A. Bohling, C. R. Abernathy, K. F. Jensen, *J. Crystal Growth,* **1994**, 136, 118.

[19] B. Q. Shi, C. W. Tu, *J. Electronic Materials*, **1999**, 28, 43.

[20] M. Imaizumi, M. Adachi, Y. Fujii, Y. Hayashi, T. Soga, T. Jimbo, M. Umeno, J. Cryst. Growth, **2000**, 221, 688.

[21] R. R. Campomanes, J. H. Dias da Silva, J. Vilcarromero, L. P. Cardoso, *J. Non-Cryst. Solids*, **2002**, 299-302, 788.

[22] P. Marchand, I. A. Hassan, I. P. Parkin, C. J. Carmalt, *Dalton Trans*, **2013**, 9406.

[23] C. E. Knapp, G. Hyett, I. P. Parkin, C. J. Carmalt, Chem. Mater., **2011**, 23, 1719.

[24] L. G. Bloor, J. Manzi, R. Binions, I. P. Parkin, D. Pugh, A. Afonja, C. S. Blackman, S. Sathasivam, C. J. Carmalt, Chem. Mater., **2012**, 24, 2864.

[25] Z. Synowiec, D. Radziewicz, I. Lindert-Zborowska, Advanced Semiconductor Devices and Microsystems., ASDAM 2000 Third International Euro Conference, 2000, 289, 293

[26] S. Sathasivam, PhD thesis, University College London 2012.

[27] L. K. Krannich, C. L. Watkins, D. K. Srivastava, *Polyhedron*, **1990**, 9, 289.

[28] C. J. Thomas, L. K. Krannich, C. L. Watkins, *Polyhedron*, **1993**, 9, 89.

[29] P. Scherrer, Gottinger Nachrichten Gesell., 1918, **2**, 98

[30] S. J. S. Qazi, A. R. Rennie, J. K. Cockcroft, M. Vickers, *J. Colloid Interface Sci.,* **2009**, 338, 105.

[31] G. Abstreiter, E. Bauser, A. Fischer, K. Ploog, *Appl. Phys.* **1978**, 16, 345

[32] I. D. Desnica, M. Ivanda, M. Kranjčec, R. Murri, N. Pinto, *J. Non-Crystalline Solid*, **1994**, **170**, 263.

[33] A. C. Adams, B. R. Pruniaux, *J. Electrochem Soc.*, 1973, **120**, 408.

[34] P. A. Betrand, *J. Vac. Sci. Technil.*, **1981**, 18, 28.

[35] S. Basharat, C. J. Carmalt, R. Binions, R. Palgrave, I. P. Parkin, *Dalton Trans*, **2008**, 591.

[36] G. Leonhardt, A. Berndtsson, J. Hedman, L. Klasson, R. Nilsson, *Phys. Status Solidi B.*, **1973**, 60, 241.